Journal of Corrosion and Materials
www.corromat.com

J. Corros. Mater. (2025) 4(2), 147–158.

Hydrogen-Driven Ru Redispersion and Ammonia-Induced Step Formation on Graphitic Nanofibres

José Mansur Assaf[1,*], Willibaldo Schmidell Netto[2]

[1] *Department of Chemical Engineering, Federal University of São Carlos, São Paulo 13565-905, Brazil*

[2] *Department of Chemical and Food Engineering, Federal University of Santa Catarina, Santa Catarina 88040-900, Brazil*

[*] Corresponding author: mansur@ufscar.br

[2] w.schmidell@ufsc.br

(Received: 21 July 2025. Received in revised form: 8 October 2025. Accepted: 23 October 2025. Published online: 30 December 2025.)

Abstract

The ammonia decomposition occurs on the dynamic Ru nanocluster surface on the graphitic nanofibre support. The activity of the catalyst depends neither on mean particle size nor on maximum Ru atom dispersion since in hydrogen and ammonia atmospheres the Ru atoms form isolated atoms, few-atom aggregates, amorphous islands, and compact nanoclusters. In this work the ammonia-induced step-edge formation of Ru nanoclusters on graphitic nanofibers is found out at 450 °C. Hydrogen activates the Ru atoms creating a Ru inventory: the total amount of single atoms, dimers, trimers grows up from 39% to 87% while the fraction of clusters falls from 61% to 13%. Ammonia recombines some part of the inventory into clusters reducing their amount up to 60% and bringing clusters back up to 40% after 3 h of exposure. On the cluster level an amorphous island with $N_{at} = 175$ and $S_{FP} = 2.35$ nm^2 is transformed into a four-layer crystalline cluster with $N_{at} = 231$ and $S_{FP} = 3.13$ nm^2. Long-term ammonia treatment yields a five-layer crystalline cluster with $N_{at} = 374$, $S_{FP} = 3.62$ nm^2, and 103.3 atoms/nm^2 staying below the approximate 4 nm^2 area limit. Thus, the catalyst becomes active due to the ammonia-induced transformation of the mobile Ru inventory into the compact clusters with numerous steps on graphitic carbon. Stepped nanoclusters provide a stable hydrogen production, not the hydrogen-induced atom reservoir or particles' growth.

Keywords: ammonia decomposition; ruthenium; graphitic nanofibres; nanoclusters; step edges; hydrogen production; identical-location microscopy.

1. Motivation and hypothesis

Ammonia is a dense hydrogen carrier which releases hydrogen without any carbon-containing products upon decomposition to nitrogen and hydrogen. Energy storage studies highlighted the use of ammonia as a hydrogen carrier for sustainable energy systems [1]. More recent evaluations highlighted ammonia's role in combustion, maritime energy and distributed fuel applications [2]. Energy transition investigations place ammonia in a carbon-neutral chemical energy economy [3]. The constraint is catalytic: high hydrogen formation has to be maintained at relatively low temperatures without loss of the metal surface responsible for N–H bond splitting and nitrogen removal.

Ruthenium belongs to the most active metals for ammonia decomposition, but the activity depends on the atomic arrangement of surface sites rather than on the absolute amount of Ru. Surface science experiments revealed Ru steps as extremely active centers for nitrogen activation [4]. Structure sensitive kinetics identified the density of such clusters as the key parameter governing ammonia synthesis turnover [5]. First-principles studies connected the elementary mechanism to the geometry of Ru surface atoms [6]. Nanoparticle investigation revealed that the role of edges and steps exceeds their relative abundance on a Ru particle [7]. Nitrogen recombination and desorption thus depend on neighboring adsorption sites and low-coordination environments. A catalyst enriched with isolated atoms is thus not necessarily the best catalyst for this reaction. Clusters of Ru atoms may become more important than maximum dispersion in case of interaction and recombination of nitrogen-containing intermediate species.

Small supported clusters pose a challenge for the interpretation. Near 1–2 nm in diameter, Ru particles cease to be simply a sphere and acquire the specific dependence of surface sites on their projection, layeredness, crystallinity and contact with the support. A disordered low island and a crystalline stepped cluster may have the same lateral size but different catalytically active surface. Describing Ru/GNF by average diameter thus removes the information necessary for the distinction of inactive spread-out islands and compact edge-bearing clusters.

Graphitic nanofibers allow to provide a carbon support which can stabilize and rearrange Ru. Basal planes, curved surfaces and edge-like binding positions appear due to the graphitic lamellae of nanofiber structure. Ru supported on

carbon nanotubes demonstrated the enhancement of ammonia decomposition [8]. Comparison of supports revealed that graphitization and metal–support contact affect Ru activity [9]. The additional effect of oxygen-containing carbon functionalities on Ru was found [10]. Recent studies linked the graphitic structure of the support to the stability of active Ru ensembles [11]. Graphitic lattice also reduces the electron microscopy background, which helps to track individual atoms and nanoclusters with high contrast.

The interface shown in Figure 1 illustrates this dual role of graphitic nanofibers. Ru atoms and clusters are not uniformly distributed on the flat support, but are present in the non-uniform carbon landscape. Edge sites and defects immobilize Ru atoms, whereas graphitic terraces allow for their motion at elevated temperatures. Such system allows for the redistribution of Ru atoms and nanoclusters under hydrogen and ammonia, but prevents unlimited lateral growth of Ru under extended ammonia decomposition.

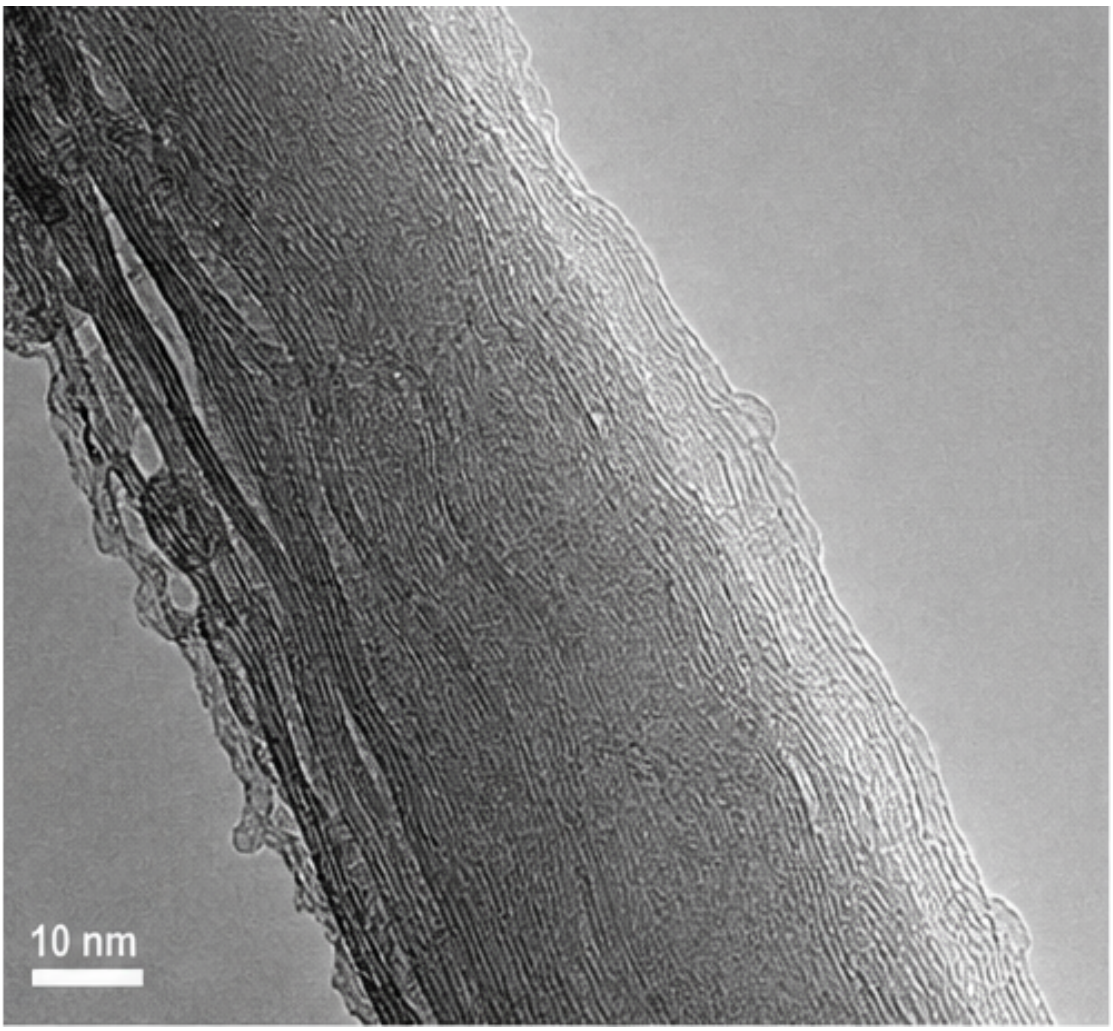

Figure 1: Ru/GNF interface.

The hypothesis about the source of increased activity during ammonia decomposition is the formation of persistent stepped Ru nanoclusters. Hydrogen provides a mobile inventory of Ru atoms, but step-enriched catalytic surface appears due to incorporation of that inventory into compact and ordered clusters by ammonia. Four parameters need to coincide: recovery of the cluster-bound Ru after hydrogen desorption, increase in the number of layers in Ru clusters, retention of the cluster footprint below 4 nm^2, and persistence of ordered stepped structures under prolonged ammonia treatment.

The hydrogen-rate curve shown in Figure 2 sets the timescale of the hypothesis. Production of hydrogen increases during initial reaction period and becomes steady afterwards. If the activity was driven by the highest amount of exposed Ru atoms, the hydrogen-rich state with numerous isolated species would dominate. The rate behavior thus indicates that the catalytic surface matures under ammonia exposure and stays active even after the restructuring period.

The rate increase thus is explained by means of structural data corresponding to the particular states. The relevant comparison is between the hydrogen-generated inventory of isolated Ru atoms and the ammonia-generated population of compact and ordered clusters. The next sections quantify the evolution of Ru population, clustering of Ru atoms, and formation of step-enriched clusters due to graphitic confinement.

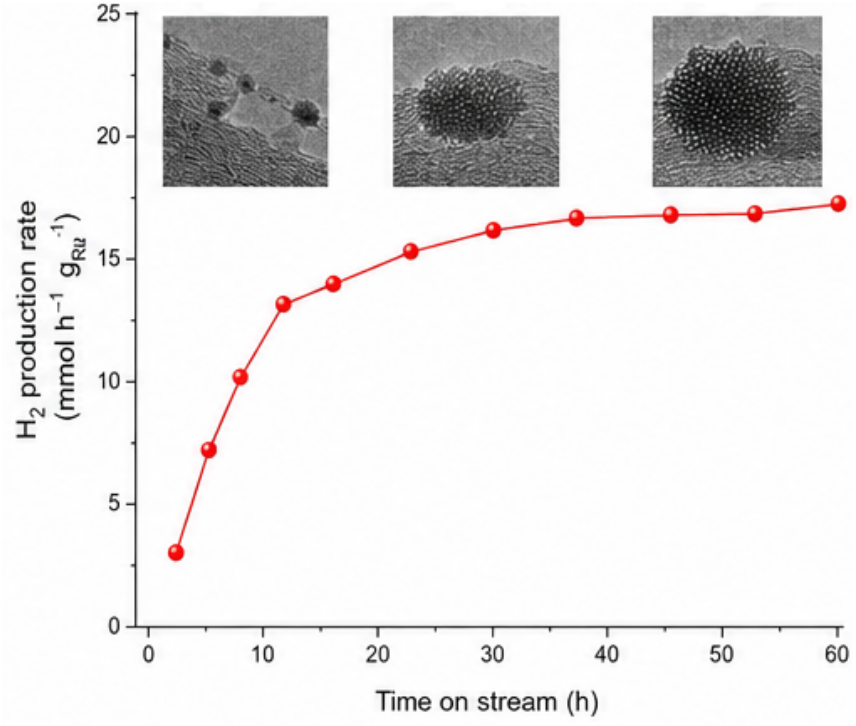

Figure 2: Hydrogen-rate maturation.

2. Ru/GNF state values and calculations

The values of Ru/GNF states used below are presented in the work of Chen et al. [12]. The record consists of the percentages of single atoms, dimers, trimers, and clusters; average nanocluster diameters; values of atom number N_{at}; footprint area S_{FP}; apparent diameter d; layer count N_l; crystallinity; atom-footprint exponents; local cluster merger events; and the ammonia decomposition rate trend. This set of values is converted into state-resolved analysis of the catalyst dedicated to step-edge generation.

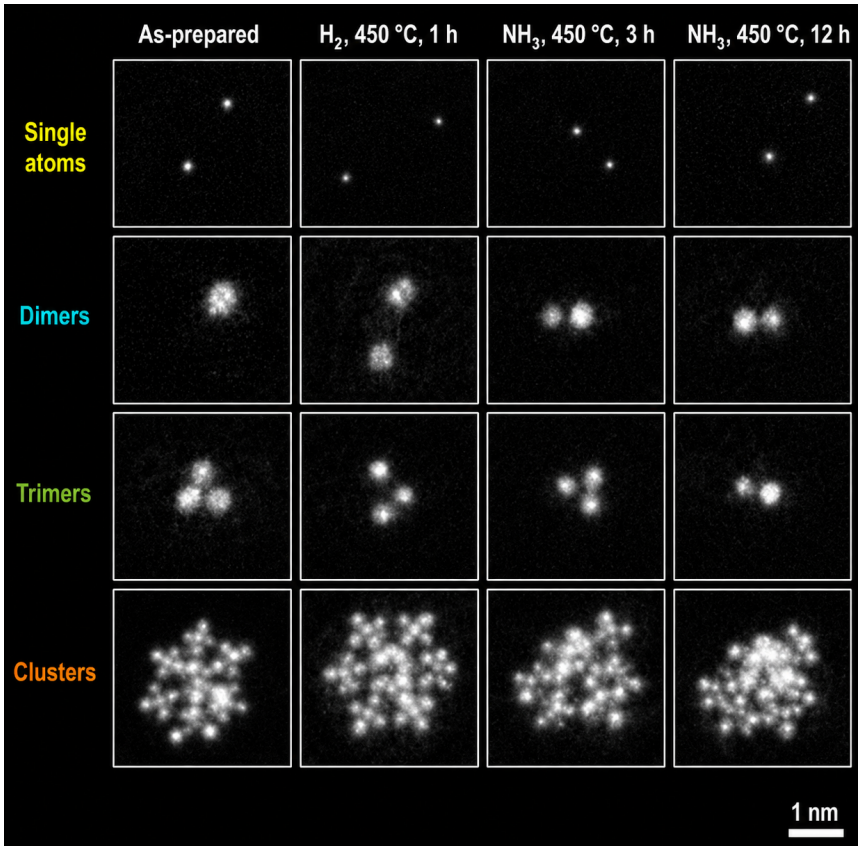

Figure 3: Thermal state record.

Figure 3 presents the sequence of experimental states. The sample begins in the as-prepared state, undergoes hydrogen treatment at 450 °C for 1 h, and ammonia treatment at 450 °C for 3 h or 12 h. The order of the visual states is deliberately chronological because hydrogen and ammonia play different roles in surface structures. Hydrogen treatment increases the non-clustered Ru fraction, while ammonia forms clusters matching the catalytic regime.

Two simple quantities are used for the analysis of the data. The non-clustered Ru fraction is

$$P_{\mathrm{nc}} = f_1 + f_2 + f_3, \tag{1}$$

where f_1, f_2, and f_3 are the percentages of single atoms, dimers, and trimers, respectively. This parameter characterizes the dominance of isolated or few-atom Ru species. It is not considered as the mass-normalized metal inventory since single atoms, dimers, and trimers have different number of atoms.

The normalized cluster density is

$$Q = \frac{N_{\mathrm{at}}}{S_{\mathrm{FP}}}. \tag{2}$$

An increase of Q means that more Ru atoms occupy the same footprint. This is the mathematical evidence of vertical densification. A cluster may increase the number of its atoms, but still be a good catalyst if the footprint of the atoms is finite and these atoms are organized in stepped layers.

The atom-footprint dependence is given by

$$N_{\mathrm{at}} \propto S_{\mathrm{FP}}^{\alpha}. \tag{3}$$

Values of α close to unity mean that the number of atoms depends mostly on the lateral size. Higher values correspond to the faster increase of the atom number compared to the footprint and reflect the development of the cluster in the third dimension. This exponent is interpreted in conjunction with crystallinity and N_l since the vertical development without forming steps is not necessarily beneficial for ammonia decomposition.

This approach makes possible to give the chemical meaning to the analyzed states. P_{nc} is the hydrogen-generated Ru inventory, P_{cl} is the cluster-bound population, Q splits the vertical densification and the lateral spreading, and α shows whether the clusters become taller or just wider. The crystallinity and N_l determine whether the densified cluster can offer step edges repeatedly.

3. Redistribution of Ruthenium Species in Gas State

The most noticeable effect is achieved under hydrogen treatment. The initial 3-hour sample contains 30% of single atoms, 7% of dimers, 2% of trimers, and 61% of clusters with 1.01 ± 0.33 nm average diameter of the cluster. Under hydrogen for 1 hour at 450 °C, the fractions of single atoms and dimers rise to 67% and 15%, respectively, trimers – to 5%, and clusters reduce to 13%. In three hours under ammonia at the same temperature, the single-atom content reduces to 47%, dimers – to 12%, trimers – to 1%, and clusters recover up to 40%. The long ammonia sample contains 42% of single atoms, 7% of dimers, 2% of trimers, and 49% of clusters after 12 hours.

Table 1: Census of Ru species.

State	Single (%)	Dimer (%)	Trimer (%)	Cluster (%)	d (nm)
As prepared, 3 h series	30	7	2	61	1.01 ± 0.33
H_2, 450 °C, 1 h	67	15	5	13	1.36 ± 0.58
NH_3, 450 °C, 3 h	47	12	1	40	1.46 ± 0.40
As prepared, 12 h series	26	6	1	67	0.93 ± 0.34
NH_3, 450 °C, 12 h	42	7	2	49	1.17 ± 0.41

The species distribution table (Table 1) allows to separate atom transportability from the stability of catalytic structures. In the hydrogen state, $P_{\mathrm{nc}} = 87\%$, which is the highest value in the whole series, but there are only 13% of clusters. The ammonia-treated state has a smaller share of non-clustered population, $P_{\mathrm{nc}} = 60\%$, and restored 40% of the clusters' fraction. The stable catalysis-based explanation cannot be based only on the isolated Ru amount, as the maximum is reached before the ammonia state appears.

The microscopy-like Ru species panel (Figure 4) proves that the categories of counted species represent the real Ru states. The single atoms can be recognized as separated bright points; dimers and trimers appear as intermediate few-atoms structures; clusters – as larger bright spots. The hydrogen treatment resulted in the domination of separated Ru species, while the ammonia treatment leaves a larger share of cluster-bound Ru. It confirms visually the numerical result

about the creation of the transportable Ru inventory under hydrogen and its restoration as multi-atom structures under ammonia.

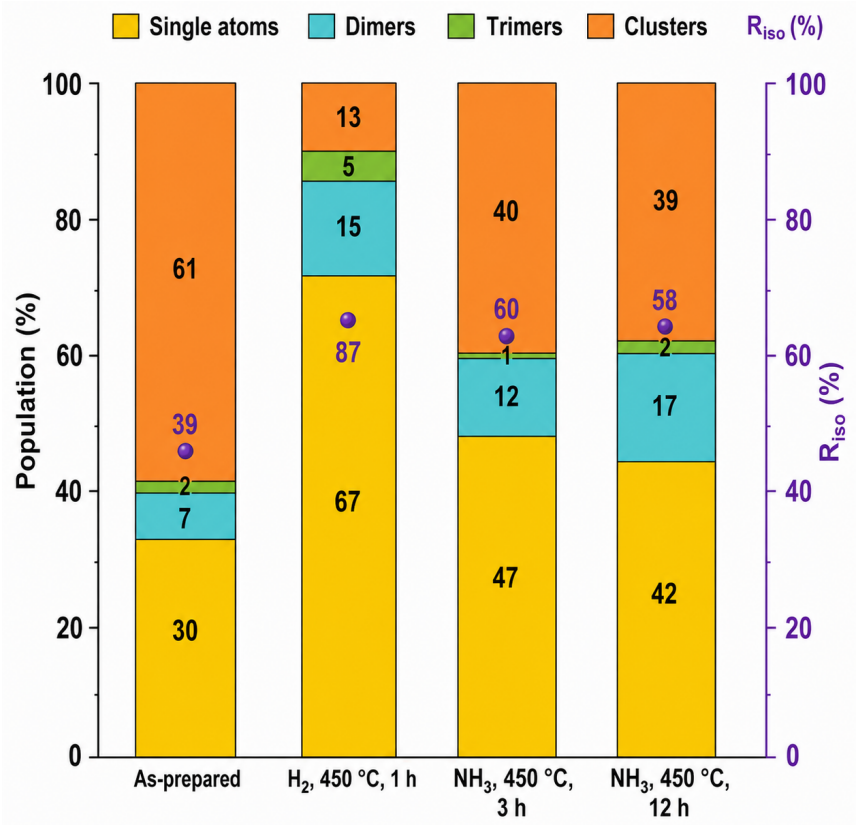

Figure 4: Ru species images.

The distribution of population is shown in Figure 5. The fraction of the clusters decreases from 61% to 13% under hydrogen and rises to 40% after ammonia. At the same time, P_{nc} varies from 39% to 87% and then to 60%. The chemical conclusion is obvious: the hydrogen treatment results in the strongest dispersion, but the ammonia treatment recovers the cluster population needed for the step edges formation.

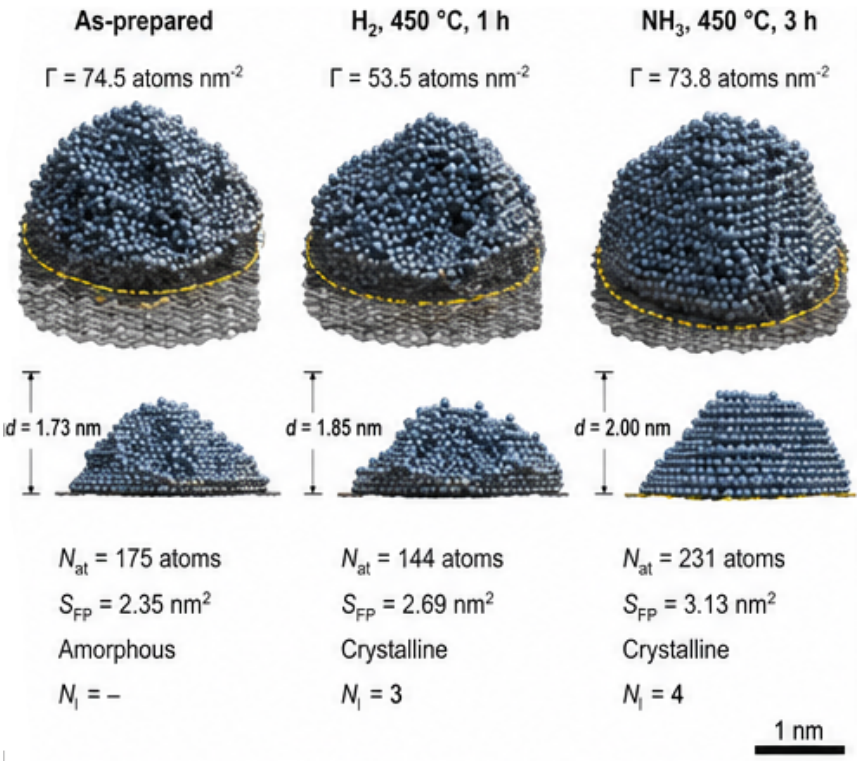

Figure 5: Population redistribution.

Average diameter alone does not give the full picture. Same-location values increase from 1.01±0.33 nm to 1.36±0.58 nm under hydrogen and to 1.46 ± 0.40 nm under ammonia. Different-location values give 0.99 ± 0.47 nm under hydrogen and 1.49 ± 0.46 nm under ammonia. Final values of the ammonia diameters are comparable, but hydrogen seems quite different when comparing the same locality.

Table 2: Evolution of the diameter by the sampling mode.

Sampling mode	As prepared (nm)	H_2, 1 h (nm)	NH_3, 3 h (nm)
Same locality	1.01 ± 0.33	1.36 ± 0.58	1.46 ± 0.40
Different localities	–	0.99 ± 0.47	1.49 ± 0.46

The numbers in Table 2 refute the possibility to explain everything only by using the information about the diameter. The catalyst may exhibit identical final average particle size despite the distinct structural pathways for atoms and clusters. For Ru/GNF, the same-location measurement is revealing in that it indicates that hydrogen affects the local Ru inventory prior to ammonia transforming some of the inventory into clusters.

4. Cluster densification and crystallographic ordering

The evolution of a single tracked Ru cluster proves the involvement of ammonia in cluster densification. The cluster starts as an amorphous island having $N_{\mathrm{at}} = 175$, $S_{\mathrm{FP}} = 2.35$ nm^2, $d = 1.73$ nm, and $Q = 74.5$ atoms nm^{-2}. Under hydrogen treatment, the same cluster achieves a crystalline three-layer state, but N_{at} reduces to 144, S_{FP} increases to 2.69 nm^2, and Q decreases to 53.5 atoms nm^{-2}. After 3 h in ammonia, the cluster evolves to $N_{\mathrm{at}} = 231$, $S_{\mathrm{FP}} = 3.13$ nm^2, $d = 2.00$ nm, four layers, and $Q = 73.8$ atoms nm^{-2}.

It is clear from the height data of Figure 6 that hydrogen and ammonia play different roles. Hydrogen induces ordering at the expense of compactness. Ammonia enhances the number of atoms, restores compactness, and increases the layer count to four. Therefore, the catalytic surface is optimized vertically rather than via the hydrogen treatment leading to maximal amount of non-clustered Ru.

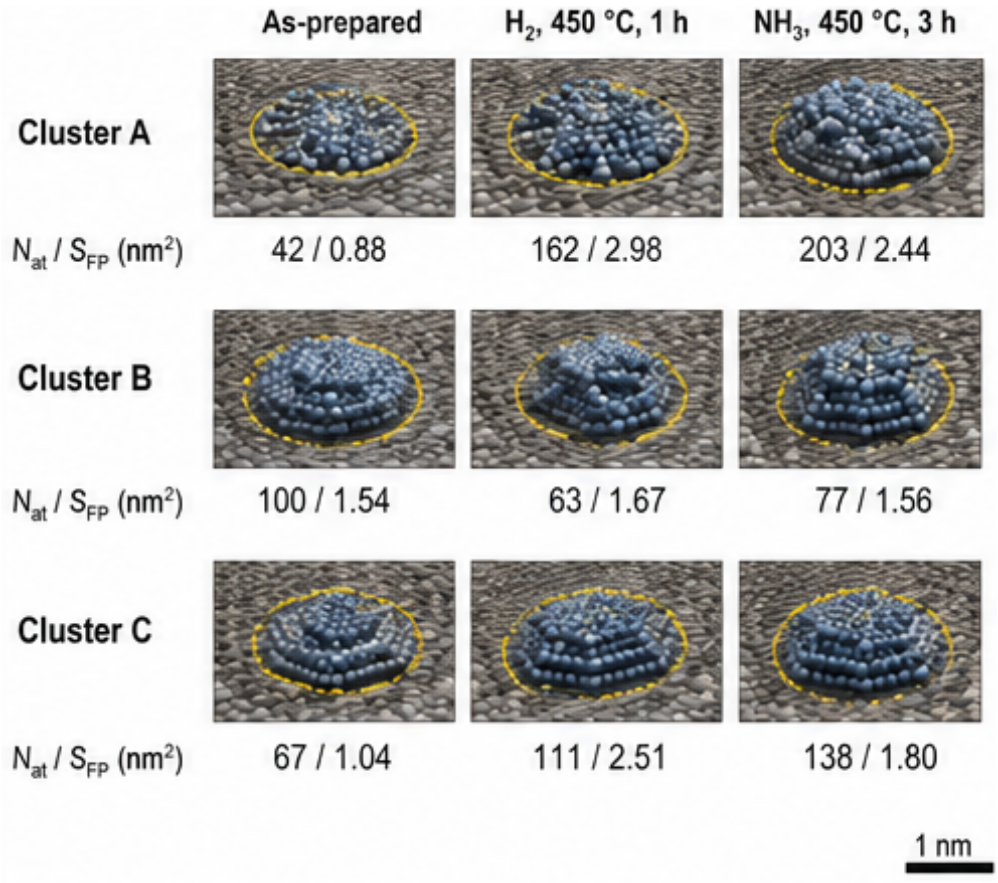

Figure 6: Single-cluster height evolution.

Table 3: Tracked cluster state values.

State	N_{at}	S_{FP} (nm^2)	d (nm)	N_l	Order	Q
As prepared	175	2.35	1.73	–	Amorphous	74.5
H_2, 450 °C, 1 h	144	2.69	1.85	3	Crystalline	53.5
NH_3, 450 °C, 3 h	231	3.13	2.00	4	Crystalline	73.8

According to the tracked values of Table 3, the ammonia-treated cluster is the first fully relevant catalytic state in the sequence. This state combines compactness with crystalline structure and four-layer configuration. A disordered cluster possesses many atoms, yet it is characterized by the lack of periodic step patterns. In contrast, a four-layer crystalline state allows presenting terraces and step edges within the limited footprint area.

Another three clusters prove the locality of the pathway under discussion. Cluster A evolves from $N_{at} = 42$ and $S_{FP} = 0.88$ nm^2 to 162 and 2.98 nm^2 under hydrogen influence, and to 203 and 2.44 nm^2 under ammonia. Cluster B evolves from 100 and 1.54 nm^2 to 63 and 1.67 nm^2 under hydrogen, and to 77 and 1.56 nm^2 under ammonia. Cluster C evolves from 67 and 1.04 nm^2 to 111 and 2.51 nm^2, and to 138 and 1.80 nm^2. All ammonia-treated clusters possess the crystalline state.

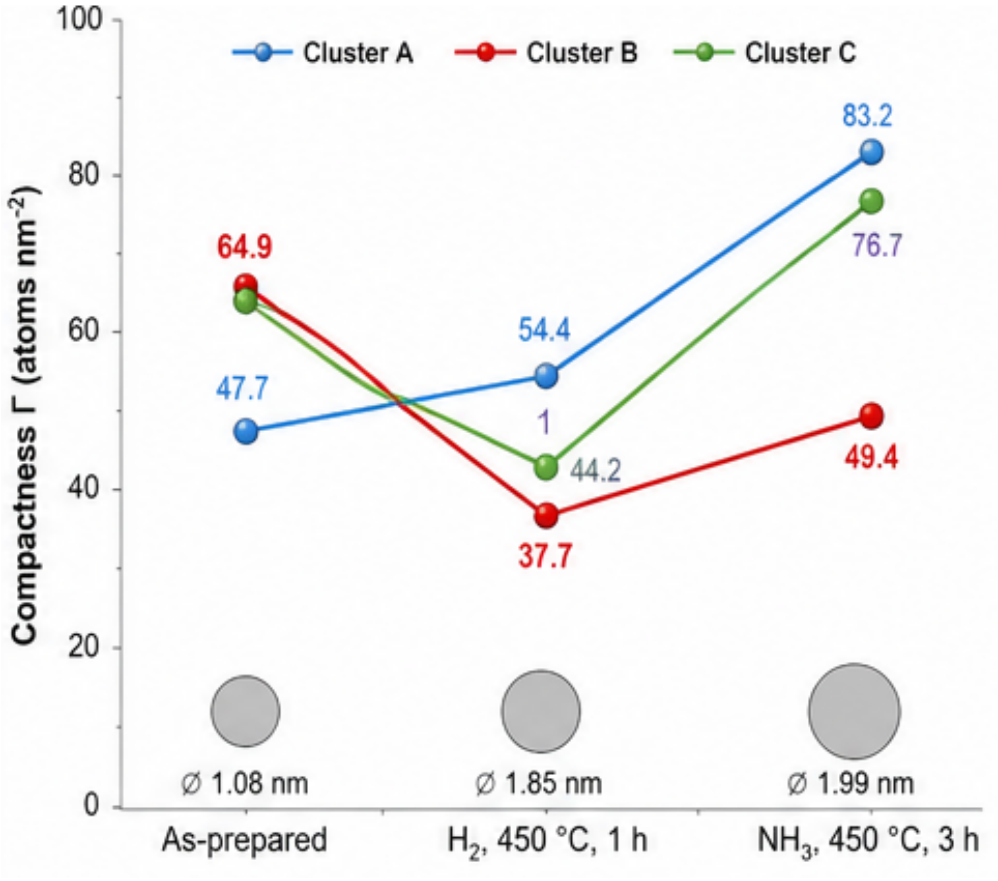

Figure 7: Three cluster pathways.

The three rows in Figure 7 show that the relevant state of the system is not the same growth pattern. Cluster A achieves significant increase in atom count and reduction of footprint after ammonia treatment. Cluster B partially restores the atom count while becoming crystalline without achieving its initial compactness. Cluster C increases the number of atoms and footprint under ammonia influence. Each pathway proves that local carbon sites and adjacent Ru species determine how completely the cluster acquires the compact crystalline state.

The compactness records in Table 4 prove ammonia-induced densification of the system as distinct from standard particle growth. Cluster A achieves the compactness of 83.2 atoms nm^{-2} under ammonia influence, and Cluster C achieves the compactness of 76.7 atoms nm^{-2}, exceeding their hydrogen-treated states. Cluster B does not become compact, which demonstrates the presence of a distribution of possible outcomes on the Ru/GNF substrate. The ensemble acquires catalytic value due to sufficient number of compact crystalline clusters rather than due to each cluster undergoing a perfect evolution pathway.

Table 4: Cluster compactness records.

Cluster	State	N_{at}	S_{FP} (nm^2)	Order	Q
A	As prepared	42	0.88	Amorphous	47.7
A	H_2, 1 h	162	2.98	Amorphous	54.4
A	NH_3, 3 h	203	2.44	Crystalline	83.2
B	As prepared	100	1.54	Amorphous	64.9
B	H_2, 1 h	63	1.67	Amorphous	37.7
B	NH_3, 3 h	77	1.56	Crystalline	49.4
C	As prepared	67	1.04	Amorphous	64.4
C	H_2, 1 h	111	2.51	Crystalline	44.2
C	NH_3, 3 h	138	1.80	Crystalline	76.7

5. Neighbour transfer, atom-footprint scaling, and twelve-hour retention

The neighbourhood events in the Ru species illustrate the process of obtaining atoms by the clusters. The Ru species are capable of transferring from one area to another, disappearing into neighbouring islands, or merging. The particular neighbour events are those where clusters 1, 2, and 3 merge into cluster 4 after hydrogen; clusters 21, 22, and 23 merge into cluster 24 after ammonia; and cluster 12 disappears whereas clusters 11, 13, and 14 gain material. Therefore, the atom feed happens from the Ru structures in the neighbourhood and not because of the development of all clusters uniformly.

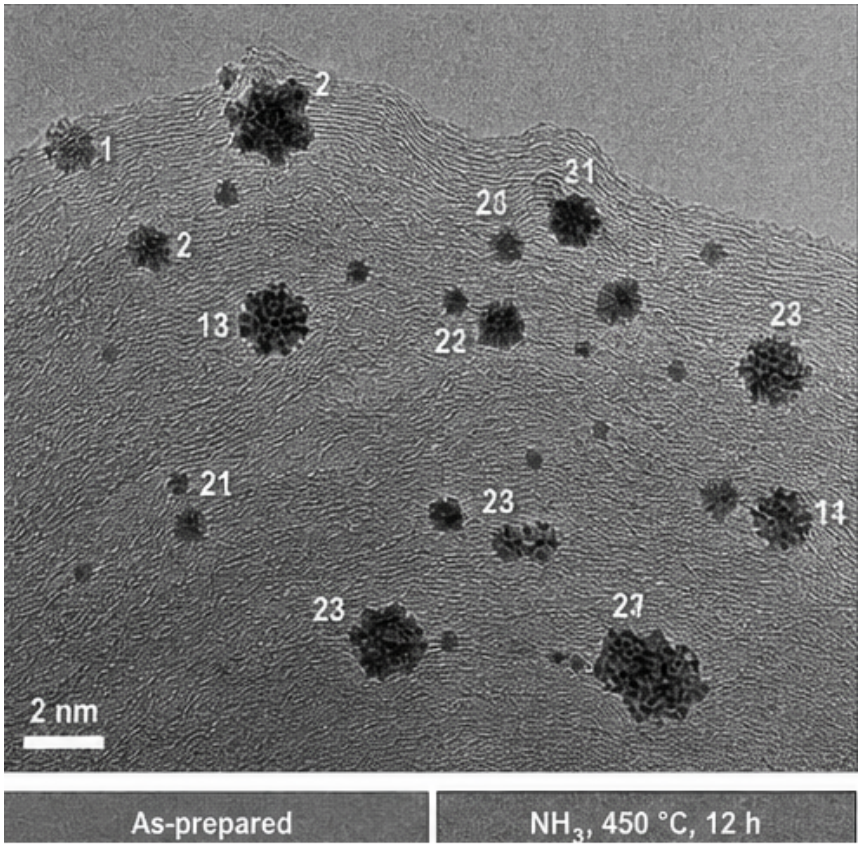

Figure 8: Local cluster neighbourhood.

The graphitic nanoreactor of the neighbourhood map in Figure 8 transforms the meaning of coalescence. The deactivation of the supported metal clusters in catalysis usually signifies coalescence. However, the limited coalescence on Ru/GNF allows forming compact islands that remain laterally constrained. Thus, the carbon nanotubes could be used as the nanoreactors of reactions, which means that they restrict the space for the metal species [13]. Moreover, the graphitic nanoreactors could alter the local transport and behaviour of the catalysts because of the confinement [14]. The direct microscopy shows the reorganisation of the metal-supported clusters under the conditions of the constrained carbon environments [15]. The confinement studies in relation to the graphitic environment indicate that the local mobility is possible under the suppression of the large-scale growth [16]. Consequently, the graphitic support offers different binding positions to the atoms so that they are capable of moving locally whereas their extension coalescence is inhibited.

The atom-footprint scaling represents the population-level approach to the same phenomenon. In region A, the value of α is changing from 1.20 in the as-prepared state to 1.01 after hydrogen and 1.57 after ammonia. In region B, it is changing

from 1.38 to 1.03 and then to 1.58. In region C, it is changing from 1.19 to 1.50 and then to 1.35. In relation to the ammonia-treated sample, the global relation is $\alpha = 1.34$ with $R^2 = 0.971$.

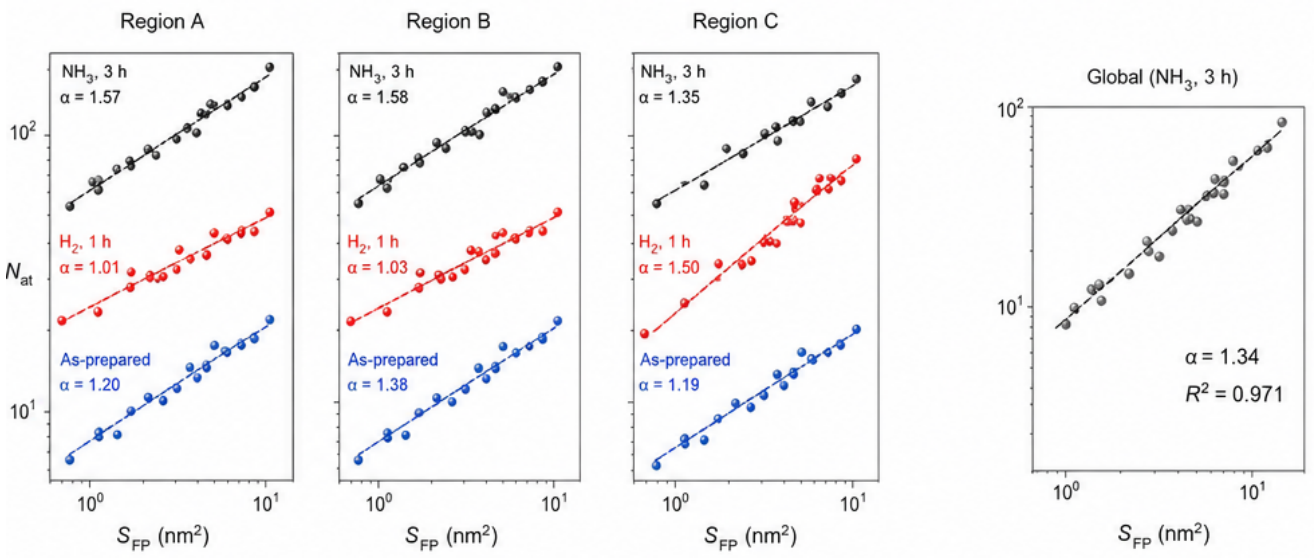

Figure 9: Atom-footprint scaling.

The log–log tendencies presented in Figure 9 show that the ammonia treatment results in enlarging of the flat Ru islands. In regions A and B, the ammonia treatment makes the value of α exceed 1.5. Hence, it means that the number of atoms becomes higher than the footprint. In region C, the ammonia treatment increases the exponent after the hydrogen treatment, making the latter elevated after the ammonia treatment as well. The ammonia global exponent confirms the tendency to three-dimensional clusters on the population level.

Table 5: Atom-footprint exponents.

Region	As prepared	H_2, 1 h	NH_3, 3 h	Structural reading
A	1.20	1.01	1.57	Vertical growth in ammonia
B	1.38	1.03	1.58	Vertical growth in ammonia
C	1.19	1.50	1.35	Early vertical growth retained
Global NH_3	–	–	1.34	Three-dimensional population trend

Thus, the exponents in Table 5 relate the increase of the number of atoms to the shape of the cluster. High α is effective only under the condition of footprint control and crystallinity. In Ru/GNF, ammonia-treated regions A and B correspond to this condition: the clusters become more three-dimensional during the same period when the hydrogen production becomes higher and steady.

Long-time ammonia test evaluates the ability of the catalyst to keep the compact crystalline state under the conditions of the reaction. A tracked cluster before the 12-h ammonia treatment contains $N_{at} = 162$, $S_{FP} = 2.63$ nm^2, $d = 1.83$ nm, amorphous order, and $Q = 61.6$ atoms nm^{-2}. After 12 h at 450 °C in ammonia, the cluster contains $N_{at} = 374$, $S_{FP} = 3.62$ nm^2, $d = 2.15$ nm, five layers, crystalline order, and $Q = 103.3$ atoms nm^{-2}.

The two-state image shown in Figure 10 represents the strongest proof of the lateral confinement. Although the number of atoms becomes twice higher, the footprint is less than 4 nm^2. The cluster does not transform into the broadened sintered particle; it becomes a five-layer crystalline island. Such shape allows preserving the step motifs in case of the ammonia decomposition.

Table 6: Twelve-hour structural state.

State	N_{at}	S_{FP} (nm^2)	d (nm)	N_l	Order	Q
As prepared	162	2.63	1.83	–	Amorphous	61.6
NH_3, 450 °C, 12 h	374	3.62	2.15	5	Crystalline	103.3

The durability aspects obtained from Table 6 form the second part of the evidence. A five-layer crystalline cluster with the parameter value of $Q = 103.3$ atoms nm^{-2} still fits into a less than 4 nm^2 footprint after 12 h. This configuration helps explain the stabilization of activity after initial activity peaks because the catalyst achieves a compact and step-rich configuration which does not require constant reconfiguration anymore.

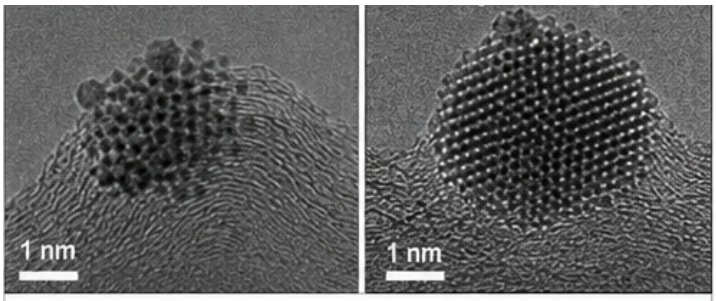

N_{at} = 162 atoms S_{FP} = 2.63 nm^2 d = 1.83 nm Amorphous Γ = 61.6 atoms nm^{-2}		N_{at} = 374 atoms S_{FP} = 3.62 nm^2 d = 2.15 nm Crystalline, N_l = 5 Γ = 103.3 atoms nm^{-2}
Population (%)		
Single atoms	26	42
Dimers	6	7
Trimers	1	2
Clusters	67	49

Figure 10: Retention of clusters in 12 h.

The presence of graphitic carbon helps achieve the required retention thanks to heterogeneity in the binding environment. In particular, microscopy studies reveal a clear difference between basal plane nucleation and edge nucleation of metal particles on the surface of graphitic materials [17]. Moreover, atomistic simulations show that factors such as curvature, vacancies and defect sites impact the binding strength of metal on carbon [18]. Ru atoms are thus able to move about locally at 450 °C, yet always get trapped by more strongly binding sites. This is not about initial immobilization, but rather about guided movement culminating in confining compact crystalline entities.

6. Catalytic interpretation

The active site model shown in Figure 11 relates the structural pattern to ammonia chemistry. While the disorderly island can have lots of exposed Ru atoms, it lacks repetition of step-edge environments. The tightly packed crystalline island has terraces, edges, and layer discontinuities where nitrogen-containing compounds can adsorb in proximity and undergo reactions. Therefore, the above discussion gives a chemical basis for increased activity when individual Ru clusters get thicker.

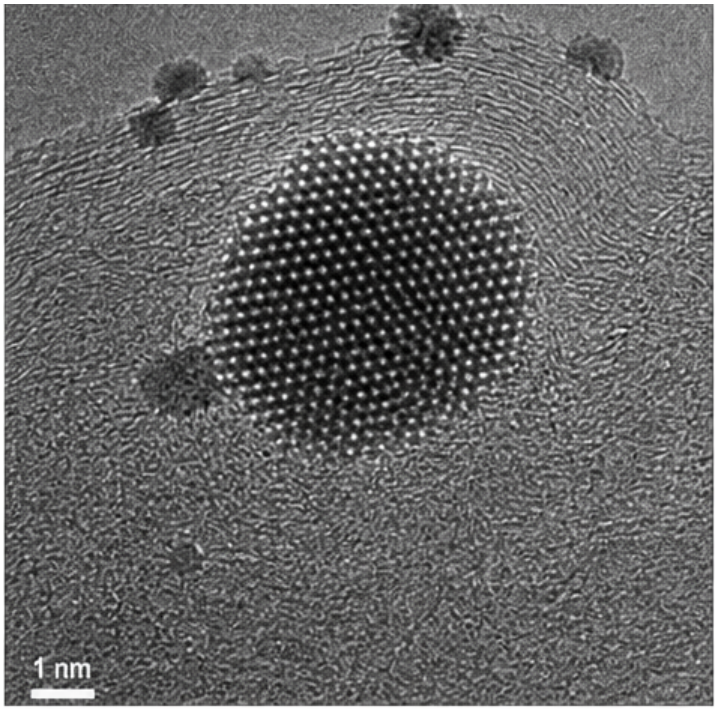

Figure 11: Ru reaction environment with steps.

The stepped environment corresponds to known Ru structure sensitivity. Experimental surface chemistry points to steps as key sites of N_2 activation on Ru [4]. Structure-sensitivity kinetic studies connect these structures to ammonia turnover [5]. Nanoparticle computations suggest that Ru morphology controls the population of catalytically important sites [19]. Density functional theory studies establish the direct relation between nitrogen chemistry and low-coordination Ru structure [20]. The size-dependent modeling additionally reveals that nanoparticle geometry determines nitrogen bond activation [21]. The step density descriptors give an effective link between nanoparticle morphology and the reaction rate [22]. The Ru/GNF provides the relevant environments only after ammonia transforms the mobile Ru into structured islands.

The structural working domain presented in Figure 12 represents the state parameters as a design goal. The 3 h ammonia cluster falls at $S_{\mathrm{FP}} = 3.13$ nm^2, $N_l = 4$, and $Q = 73.8$ atoms nm^{-2}. The 12 h ammonia cluster falls at $S_{\mathrm{FP}} = 3.62$ nm^2, $N_l = 5$, and $Q = 103.3$ atoms nm^{-2}. The ammonia-treated Clusters A, B, and C fall at $S_{\mathrm{FP}} = 2.44$, 1.56, and 1.80 nm^2, respectively, with compactness of 83.2, 49.4, and 76.7 atoms nm^{-2}.

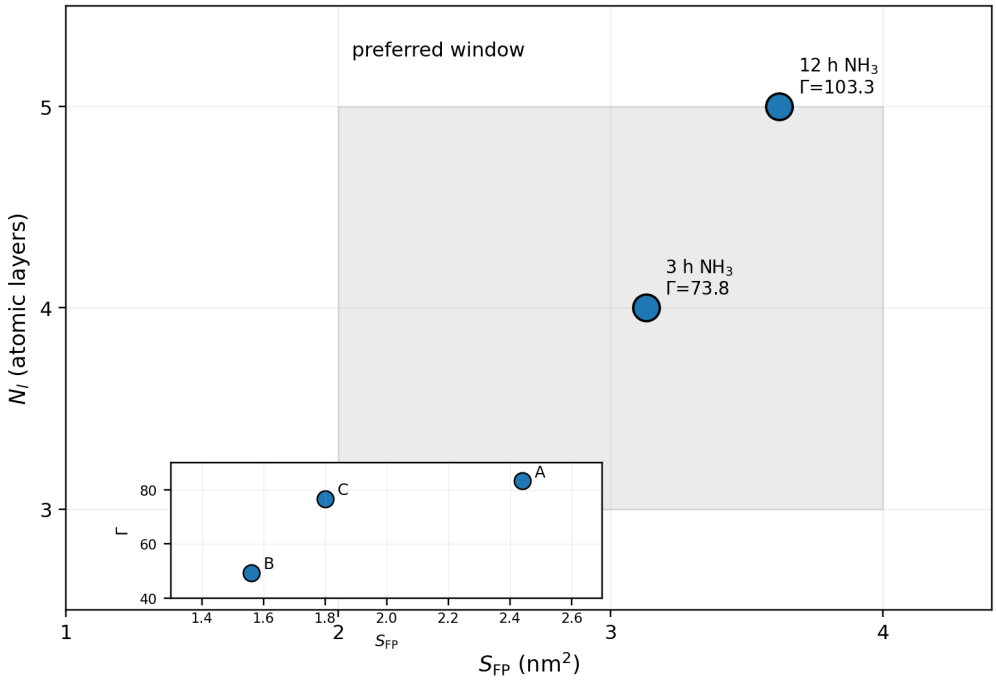

Figure 12: Layer-footprint domain.

The domain plot shows the morphology of the Ru/GNF as a laterally limited crystalline cluster rather than the minimum available Ru particle. The robust tracked states remain below approximately 4 nm^2 while having from four to five layers. The smaller ammonia-treated clusters can also be compact and crystalline, but the most durable state represents the limited footprint along with vertical structure. That is the morphological property that correlates well with the maturation of hydrogen rates.

The entire process provides for a separate function for each step of the gas. Hydrogen raises P_{nc}, forms a mobile Ru stock, and ammonia lowers the number of non-clustered particles, regenerates cluster-bound Ru, raises crystallinity, and forms layered islands. This conversion can be carried out due to graphitic nanofibers which have high atom mobility along with effective trapping of atoms on certain carbon centers. This means that Ru/GNF becomes active by the nature of step-edge assemblies instead of maximum dispersion.

7. Conclusion

The Ru/GNF state record addresses the catalytic hypothesis directly. The initial rise in hydrogen yield on ammonia dissociation does not depend on the maximal isolated-Ru concentration. It occurs when the latter equals 87%, with the cluster concentration being just 13%. The active catalyst state emerges when the ammonia molecule transforms some part of the mobile Ru metal into compact crystalline clusters. After 3 hours in ammonia environment, P_{nc} reduces to 60%, the cluster concentration goes up to 40%, and one particular tracked cluster attains the parameters of $N_{\mathrm{at}} = 231$, $S_{\mathrm{FP}} = 3.13$ nm^2, and four atomic layers. At 12 hours, the tracked cluster has $N_{\mathrm{at}} = 374$, $S_{\mathrm{FP}} = 3.62$ nm^2, and five atomic layers, remaining under the approximate 4 nm^2 footprint limit.

Hence, the active Ru/GNF catalyst state comprises a population of compact, laterally constrained, crystalline nanoclusters with persistent step-edge sites. Hydrogen is responsible for the atom-mobilizing stage, while ammonia takes care of

the step-forming stage. Graphitic nanofibres provide durability of such stages owing to the possibility of the local Ru atom mobility and restriction of the lateral growth of the clusters. The hydrogen yield rises due to ammonia conversion of mobile Ru metal into edge-bearing nanoclusters appropriate for nitrogen recombination.

Conflicts of interest

The author declares no conflict of interest.

References

[1] Klerke, A., Christensen, C. H., Nørskov, J. K., & Vegge, T. (2008). Ammonia for hydrogen storage: challenges and opportunities. Journal of Materials Chemistry, 18(20), 2304-2310.

[2] Valera-Medina, A., Xiao, H., Owen-Jones, M., David, W. I., & Bowen, P. J. (2018). Ammonia for power. Progress in Energy and combustion science, 69, 63-102.

[3] MacFarlane, D. R., Cherepanov, P. V., Choi, J., Suryanto, B. H., Hodgetts, R. Y., Bakker, J. M., ... & Simonov, A. N. (2020). A roadmap to the ammonia economy. Joule, 4(6), 1186-1205.

[4] Dahl, S., Logadottir, A., Egeberg, R. C., Larsen, J. H., Chorkendorff, I., Törnqvist, E., & Nørskov, J. K. (1999). Role of steps in N 2 activation on Ru (0001). Physical Review Letters, 83(9), 1814.

[5] Jacobsen, C. J., Dahl, S., Hansen, P. L., Törnqvist, E., Jensen, L., Topsøe, H., ... & Chorkendorff, I. (2000). Structure sensitivity of supported ruthenium catalysts for ammonia synthesis. Journal of Molecular Catalysis A: Chemical, 163(1-2), 19-26.

[6] Honkala, K., Hellman, A., Remediakis, I. N., Logadottir, A., Carlsson, A., Dahl, S., ... & Nørskov, J. K. (2005). Ammonia synthesis from first-principles calculations. science, 307(5709), 555-558.

[7] Hansgen, D. A., Vlachos, D. G., & Chen, J. G. (2010). Using first principles to predict bimetallic catalysts for the ammonia decomposition reaction. Nature chemistry, 2(6), 484-489.

[8] Yin, S. F., Xu, B. Q., Zhu, W. X., Ng, C. F., Zhou, X. P., & Au, C. T. (2004). Carbon nanotubes-supported Ru catalyst for the generation of COx-free hydrogen from ammonia. Catalysis Today, 93, 27-38.

[9] García-García, F. R., Álvarez-Rodríguez, J., Rodríguez-Ramos, I., & Guerrero-Ruiz, A. (2010). The use of carbon nanotubes with and without nitrogen doping as support for ruthenium catalysts in the ammonia decomposition reaction. Carbon, 48(1), 267-276.

[10] Garcia-Garcia, F. R., Gallegos-Suarez, E., Fernandez-Garcia, M., Guerrero-Ruiz, A., & Rodriguez-Ramos, I. (2017). Understanding the role of oxygen surface groups: The key for a smart ruthenium-based carbon-supported heterogeneous catalyst design and synthesis. Applied Catalysis A: General, 544, 66-76.

[11] Mazzone, S., Goklany, T., Zhang, G., Tan, J., Papaioannou, E. I., & García-García, F. R. (2022). Ruthenium-based catalysts supported on carbon xerogels for hydrogen production via ammonia decomposition. Applied Catalysis A: General, 632, 118484.

[12] Chen, Y., Young, B. J., Aliev, G. N., Kordatos, A., Popov, I., Ghaderzadeh, S., ... & Khlobystov, A. N. (2025). Evolution of amorphous ruthenium nanoclusters into stepped truncated nano-pyramids on graphitic surfaces boosts hydrogen production from ammonia. Chemical Science, 16(6), 2648-2660.

[13] Rance, G. A., Solomonsz, W. A., & Khlobystov, A. N. (2013). Click chemistry in carbon nanoreactors. Chemical Communications, 49(11), 1067-1069.

[14] del Carmen Gimenez-Lopez, M., Kurtoglu, A., Walsh, D. A., & Khlobystov, A. N. (2016). Extremely stable platinum-amorphous carbon electrocatalyst within hollow graphitized carbon nanofibers for the oxygen reduction reaction. Adv. Mater, 28(41), 9103-9108.

[15] Lodge, R. W., Rance, G. A., Fay, M. W., & Khlobystov, A. N. (2018). Movement of palladium nanoparticles in hollow graphitised nanofibres: the role of migration and coalescence in nanocatalyst sintering during the Suzuki–Miyaura reaction. Nanoscale, 10(40), 19046-19051.

[16] Cao, K., Biskupek, J., Stoppiello, C. T., McSweeney, R. L., Chamberlain, T. W., Liu, Z., ... & Kaiser, U. (2020). Atomic mechanism of metal crystal nucleus formation in a single-walled carbon nanotube. Nature Chemistry, 12(10), 921-928.

[17] Sutter, P. W., Flege, J. I., & Sutter, E. A. (2008). Epitaxial graphene on ruthenium. Nature materials, 7(5), 406-411.

[18] A. Z. Jovanovic, S. V. Mentus, N. V. Skorodumova and I. A. Pasti, Reactivity screening of single atoms on modified graphene surface: from formation and scaling relations to catalytic activity, *Advanced Materials Interfaces*, 2021, *8*, 2001814.

[19] Hayashi, F., Toda, Y., Kanie, Y., Kitano, M., Inoue, Y., Yokoyama, T., ... & Hosono, H. (2013). Ammonia decomposition by ruthenium nanoparticles loaded on inorganic electride C12A7: e^-. Chemical Science, 4(8), 3124–3130.

[20] Gavnholt, J., & Schiøtz, J. (2008). Structure and reactivity of ruthenium nanoparticles. Physical Review B—Condensed Matter and Materials Physics, 77(3), 035404.

[21] Arevalo, R. L., Aspera, S. M., Sison Escaño, M. C., Nakanishi, H., & Kasai, H. (2017). First principles study of methane decomposition on B5 step-edge type site of Ru surface. Journal of Physics: Condensed Matter, 29(18), 184001.

[22] Casey-Stevens, C. A., Lambie, S. G., Ruffman, C., Skúlason, E., & Garden, A. L. (2019). Geometric and electronic effects contributing to N2 dissociation barriers on a range of active sites on Ru nanoparticles. The Journal of Physical Chemistry C, 123(50), 30458-30466.